Computer Modeling in Engineering & Sciences
DOI:10.32604/cmes.2020.09778
Article

Innovative Design and Additive Manufacturing of Regenerative Cooling Thermal Protection System Based on the Triply Periodic Minimal Surface Porous Structure

Xinglong Wang[1,2], Cheng Wang[1,2], Xin Zhou[1,*], Mingkang Zhang[3], Peiyu Zhang[1] and Lei Wang[2]

[1]Science and Technology on Plasma Dynamics Laboratory, Air Force Engineering University, Xi'an, 710038, China
[2]Basic Department, Air Force Engineering University, Xi'an, 710051, China
[3]School of Mechanical & Automotive Engineering, South China University of Technology, Guangzhou, 510640, China
*Corresponding Author: Xin Zhou. Email: dr_zhouxin@126.com
Received: 18 January 2020; Accepted: 04 March 2020

Abstract: The new regenerative cooling thermal protection system exhibits the multifunctional characteristics of load-carrying and heat exchange cooling, which are fundamental for the lightweight design and thermal protection of hypersonic vehicles. Triply periodic minimal surface (TPMS) is especially suitable for the structural design of the internal cavity of regenerative cooling structures owing to its excellent structural characteristics. In this study, test pieces were manufactured using Ti6Al4V lightweight material. We designed three types of porous test pieces, and the interior was filled with a TPMS lattice (Gyroid, Primitive, I-WP) with a porosity of 30%. All porous test pieces were manufactured via selective laser melting technology. A combination of experiments and finite element simulations were performed to study the selection of the internal cavity structure of the regenerative cooling thermal protection system. Hence, the relationship between the geometry and mechanical properties of a unit cell is established, and the deformation mechanism of the porous unit cell is clarified. Among the three types of porous test pieces, the weight of the test piece filled with the Gyroid unit cell was reduced by 8.21%, the average tensile strength was reduced by 17.7% compared to the solid test piece, while the average tensile strength of the Primitive and I-WP porous test pieces were decreased by 30.5% and 33.3%, respectively. Compared with the other two types of unit cells, Gyroid exhibited better mechanical conductivity characteristics. Its deformation process was characterised by stretching, shearing, and twisting, while the Primitive and I-WP unit cells underwent tensile deformation and tensile and shear deformation, respectively. The finite element predictions in the study agree well with the experimental results. The results can provide a basis for the design of regenerative cooling thermal protection system.

Keywords: Triply periodic minimal surface (TPMS); regenerative cooling thermal protection system; selective laser melting; mechanical properties; fracture analysis

1 Introduction

A regenerative cooling thermal protection system [1] is an important component of hypersonic aircraft [2], and its complex internal cavity structure (including flow channels and porous load-carrying structures such as honeycomb and foam) has garnered significant research attention. The inner cavity structure of the early regenerative cooling thermal protection structure has been primarily designed by combining a honeycomb sandwich load-bearing structure and a D-shaped cooling tube [3–4]. In this design mode, the cooling pipe exhibits poor compatibility with the honeycomb sandwich, which will hinder the transmission of shear loads to the interior during absorption of excess heat, causing thermal strain in the entire sandwich structure.

The internal cavity structure of the new regenerative cooling thermal protection structure is designed according to the bionic bone structure [5–6], combined with an aircrafts load-carrying structure design and thermal protection design. The interior of an aircraft's load-carrying parts is filled with a porous structure, and the cooling channels formed by the porous structures interconnecting each other are used as a platform for a cooling medium attachment and convection heat exchange, replacing the cooling pipeline in the first-generation design. The new design integrates the load-bearing and heat exchange cooling function of the porous structure [7]. Under the premise of ensuring the integrity of the mechanical properties of an aircraft's load-bearing components, this new idea reduces the weight of the structure and offers the new function of diversion and heat transfer to the internal cavity channel, which maximises the function of the porous structure and can be regarded as a bionic design.

This type of bionic structure is difficult to manufacture using traditional machining methods. Additive manufacturing technology can produce alloy structures with complex microscopic morphologies [8–9], which allows the materials to be shaped into different-scale structures (bionic structure). The additive manufacturing bionic structure is a hot topic and numbers of works have been published recently. Peng et al. characterize a novel bionic design and fabrication process for porous implants [10]. Arabnejad et al. present an intuitive visualization method to understand the relationship of cell topology, pore size, porosity with constraints imposed by bone ingrowth requirements [11]. During additive manufacturing, special attention must be paid to defects such as surface pore caused by the bubbles on the melt pool surface [12]. Selective laser melting (SLM) technology, as a mature additive manufacturing technology [13], offers the advantages of high forming accuracy and relatively low cost, and it has been applied in this study.

Under the new design, researchers have tested different porous structures, such as foam and truss-like lattice [14], as the internal cavity structure of the regenerative cooling structure. Among them, the foam structure exhibits the characteristics of disorder, such that the oil flowing in the inner cavity channel is subjected to a greater resistance and cannot flow normally [15]; meanwhile, the truss-like lattice structure is affected by its own gravity. The size of the overhang section and the angle from the horizontal are limited in additive manufacturing [16]; therefore, free design of the internal cavity structure cannot be achieved.

A triple periodic minimal surface (TPMS) [17] can effectively solve the problems above. As a minimal surface, the average curvature of each point on the TPMS is zero; the surface is smooth and no sharp corners exist, and the holes are mutually connected [18–19]. These beneficial structural characteristics can ensure the smooth flow of the cooling medium in the porous channel. In addition, the TPMS can achieve the precise control of the pore size and shape by modifying the TPMS implicit function expression parameters [20]. It is particularly suitable for the application requirements of the internal support of an aircraft load-carrying structure. During the SLM manufacturing, the TPMS porous structure exhibits self-supported characteristics [16], meaning that the previously produced layer can almost support the next layer, without the demands of adding additional support structures, which can realise the integrated moulding of

the internal cavity structure. This self-supported property enables more complicated internal cavity structures to be manufactured [21]. These advantages show that the TPMS porous structure is more suitable for the internal cavity structure design of the regenerative cooling structure.

The emphasis of this study is on the design and additive manufacturing of new regenerative cooling structure simulation parts for hypersonic aircraft. SLM technology and Ti6Al4V lightweight materials were used and two key research points were emphasized: lightweight design and integrity of mechanical properties. The research began from the simplest load-bearing environment, i.e., the tensile load. We designed three types of TPMS porous test pieces, i.e., Gyroid, Primitive, and I-WP for SLM manufacturing, finite element simulations, and tensile experiments, respectively. Micromorphology analysis was performed on the fracture surface of the test piece using scanning electron microscopy (SEM). Based on the experiment, we analysed the differences in mechanical properties of the three porous structures and their causes. This study involves the porous structure selection of the regenerative cooling structure and provides a basis for the design of regenerative cooling thermal protection systems.

2 Design of TPMS Porous Structure

The surface equations of the TPMS test pieces (Gyroid, Primitive, and I-WP) were input into Autodesk Netfabb Standard, a commercial modelling software, to construct their porous unit cells. Porous unit cells with different porosities can be obtained by setting different wall thicknesses. The Gyroid, Primitive, and I-WP surfaces can be expressed by the following implicit formulas:

$$F_G(x,y,z) = \cos(p_x x)\sin(p_y y) + \cos(p_y y)\sin(p_z z) + \cos(p_z z)\sin(p_x x) \tag{1}$$

$$F_P(x,y,z) = \cos(p_x x) + \cos(p_y y) + \cos(p_z z) \tag{2}$$

$$F_{I-WP}(x,y,z) = \cos(p_x x)\cos(p_y y) + \cos(p_y y)\cos(p_z z) + \cos(p_z z)\cos(p_x x) \tag{3}$$

For the equation above, p_i is the TPMS function period, which is defined as:

$$p_i = 2\pi\frac{n_i}{L_i}(i = x,y,z) \tag{4}$$

where n_i is the number of unit cell repetitions in the x, y, and z directions; L_i is the absolute size of the unit cell in these directions.

The obtained unit cell model is shown in Figs. 1(a)–1(c). To ensure the fluidity of the cooling medium in the internal cavity of the regenerative cooling structure, and that the strength of the aircraft load-carrying structure does not change in magnitude, the porosity of the unit cell was designed to be 30% and the unit cell size was 2 mm × 2 mm × 2 mm. According to the research of Maskery et al. [20], the unit cell repeat number of 4 × 4 × 4 and above can effectively eliminate the size effect on the structure performance of the unit cell. Therefore, the planar array of the unit cells in this study was 4 × 4, and the section size was 8 mm × 8 mm. The wall thickness of the shell of the tensile test piece was designed to be 1.5 mm, with a machining allowance of 0.5 mm. In summary, the diameter of the tensile test piece was 11 mm. According to ISO 6892-1 [22], a proportional relationship exists between the gauge length and diameter of the tensile test piece of $L_0 = 5d_0$. Therefore, we set the TPMS porous unit cell array as 4 × 4 × 28 to obtain a porous block and intersected it with a cylinder measuring Φ8 × 55 by a Boolean operation. The designed porous cylinder is shown in Figs. 1(d)–1(f).

The TPMS porous cylinder was combined with the shell of the tensile test piece to obtain the STL format geometric model that was finally used for the finite element simulation and SLM manufacturing. The dimensions of the remaining parts of the tensile test piece are marked in Fig. 2. It is noteworthy that the

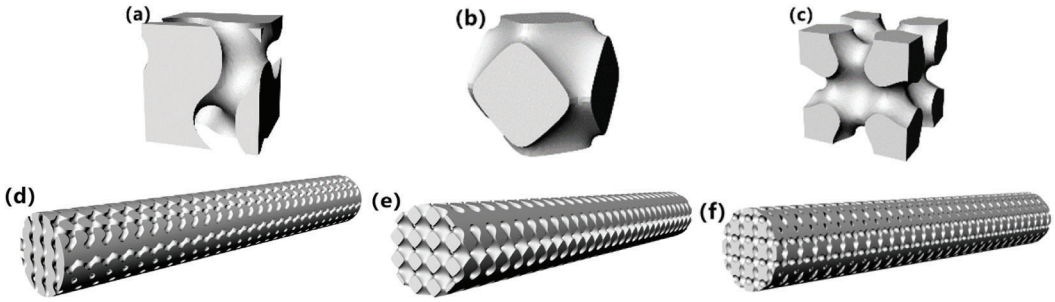

Figure 1: Individual Gyroid, Primitive, and I-WP unit cell with $\rho^* = 0.7$ are shown in (a), (b), and (c), respectively; cylindrical lattice structures comprising 4 × 4 × 28 unit cells are shown in (d), (b), and (f)

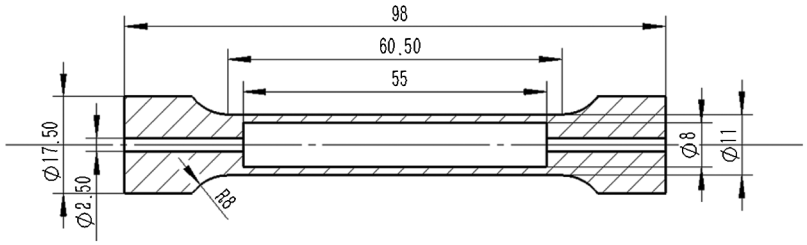

Figure 2: Size of tensile test piece

holes measuring are powder outlet holes for cleaning the unmelted powder remaining in the structure after SLM manufacturing.

3 Experimental Method

3.1 Experimental Equipment, Materials, and Processes

According to the design dimensions of the tensile test pieces, three types of TPMS porous structures and solid tensile test piece samples were manufactured via SLM manufacturing technology. To ensure sufficient experimental samples, three samples were prepared for each type, in which Ti6Al4V was used as the experimental material. The manufacturing platform was a DEMETAL-100 machine. To avoid the bending of the test piece caused by thermal stress concentration during processing, vertical printing was adopted. The SLM processing parameters are shown in Tab. 1. All specimens were prepared in an argon atmosphere with oxygen content below 100 ppm.

The powder was analysed before SLM manufacturing, and the d10, d50, and d90 powder particles based on the particle size distribution measured 20, 33, and 44 μm, respectively. The manufactured tensile test specimens are shown in Fig. 3.

3.2 Mechanical Testing and Microstructure Analysis

A uniaxial tensile test was performed on the test specimens using a CMT-5105 universal testing device equipped with a 100 kN load cell to evaluate the tensile properties of the solid and TPMS porous test pieces. The deformation rate was 0.6 mm/min. The mechanical properties of the solid and three types of TPMS porous test pieces were obtained experimentally. Prior to commencing the experiment, the gauge length of the test piece was marked, and the diameter was measured. After the test, the elongation and diameter of the fracture location were measured, and the experimental results, such as the percentage elongation and percentage in reduced area of the test piece, were calculated.

Table 1: SLM parameters used in the production of TPMS porous tensile test piece for mechanical testing

SLM parameter	
Laser power	170 W
Laser scan speed	1200 mm/s
Laser hatch spacing	65 μm
Power deposition thickness	30 μm
Spot diameter	50 μm

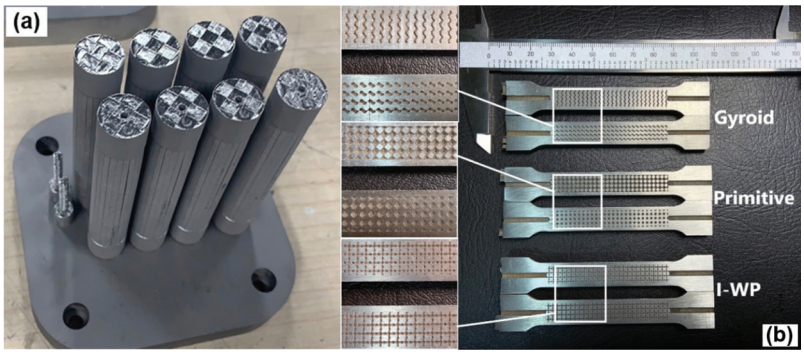

Figure 3: Gyroid, Primitive and I-WP porous test pieces manufactured by SLM are shown in Fig. 3a; Fig. 3b shows the internal structure of the three types of test pieces

To obtain further experimental results, micro-morphology analysis was performed on the fracture by SEM. First, we captured a photograph of the overall shape of the fracture to study the macroscopic morphology and subsequently analysed the characteristics of the local fault.

4 Results and Discussion

4.1 Quality Analysis of SLM Manufacturing Test Pieces

After SLM manufacturing, post-processing operations such as wire cutting, surface polishing, and cleaning excess powder were performed on the test pieces. Subsequently, all the test pieces were weighed and compared with the design mass. The calculated mass reduction percentage is shown in Tab. 2. The design masses of the solid and TPMS porous test pieces were 46.701 and 42.922 g, respectively. It is noteworthy that the mass of the Primitive test piece is significantly higher than that of the other two test pieces. Micro-scale pores appeared in porous cylinder owing to the characteristics of the Primitive's own structure, causing some powders to be non-removable and hence remained inside the porous structure of the test piece. Additionally, as shown in Fig. 3b, the metal powder that was not completely melted during SLM manufacturing adhered to the surface of the porous structure. The unmelted metal powder and the lathe processing errors contributed to the mass error of the test piece. From the research of Gümrük et al. [23], the incompletely melted metal powder that adhered to the surface of the porous structure would affect the overall performance of the test piece.

4.2 Analysis of Tensile Test Results

4.2.1 Finite Element Analysis

In this study, Simsolid meshless finite element analysis software was used to perform a linear elastic statics simulation analysis on the designed test piece to simulate the mechanical properties of the elastic

Table 2: Quality analysis of the solid, Gyroid, Primitive, and I-WP tensile test pieces manufactured by SLM

The sample number	Mass of specimen/g	Average mass of specimen/g	Percentage mass reduction
Original 1	46.190	46.275	
Original 2	46.436		
Original 3	46.276		
Gyroid 1	42.283	42.477	8.21%
Gyroid 2	42.603		
Gyroid 3	42.547		
Primitive 1	43.932	43.658	5.66%
Primitive 2	43.506		
Primitive 3	43.538		
I-WP 1	42.356	42.367	8.45%
I-WP 2	42.227		
I-WP 3	42.518		

section of the test piece. We need to establish a connection between the inner porous cylinder and the test piece shell after importing the geometric model, and then set the model material parameters and the boundary conditions to solve. When setting the boundary conditions, the clamping end of one side of the test piece was fixed, and the displacement load of 0.2 mm was set at the other end. The obtained von Mises stress cloud diagrams of the solid, Gyroid, Primitive, and I-WP porous test pieces are shown in Fig. 4. As shown, under the same displacement load, the test piece filled with the Gyroid unit cell has a higher von Mises stress level and more uniform stress distribution than the other two test pieces. Compared with the solid test piece, the von Mises stress of the Gyroid, Primitive, and I-WP porous test pieces decreased by 17.5%, 39.8%, and 40.7%, respectively. This indicates that the test piece filled with the Gyroid unit cell can maintain a relatively complete strength level while reducing the weight, thereby making it more suitable for the internal cavity design of the regenerative cooling structure. Furthermore, the stress cloud diagram shows that the maximum stress point of the test piece filled with the porous unit cells (Gyroid, Primitive, and I-WP) appears at the junction of the porous structure and the test piece shell, and that it is close to the powder outlet, thereby indicating that the joint will likely exhibit a stress concentration. Therefore, the test piece is expected to break at the joint, thereby necessitating special attention.

In the 3 × 3 × 3 lattice simulation experiment, the displacement load was set to 0.012 mm. Comparing Figs. 5a, 5c, and 5e, it is clear that among the three types of porous unit cells, Gyroid exhibits the highest stress level and more uniform stress distribution, and its deformation behaviour is similar to that of traditional cellular solids, such as random foams, which can effectively disperse axial loads and has better bearing capacity. It is clear from Fig. 5d that the stress of the Primitive lattice is primarily concentrated in the thin neck region where the unit cell is connected, and the stress of the I-WP lattice is primarily concentrated in the thin column area of the unit cell itself, as shown in Fig. 5f. The analysis shows that under the action of an axial load, these weak areas will enter the plastic area first, and it is preliminarily judged that the failure of the porous structure may occur at the corresponding stress concentration location.

4.2.2 Analysis of Tensile Test Data

Before presenting the tensile stress-strain curve of the TPMS porous test piece, the meaning of the abscissa and ordinate axes must be explained. The abscissa axis ‘strain’ in Fig. 6a represents the

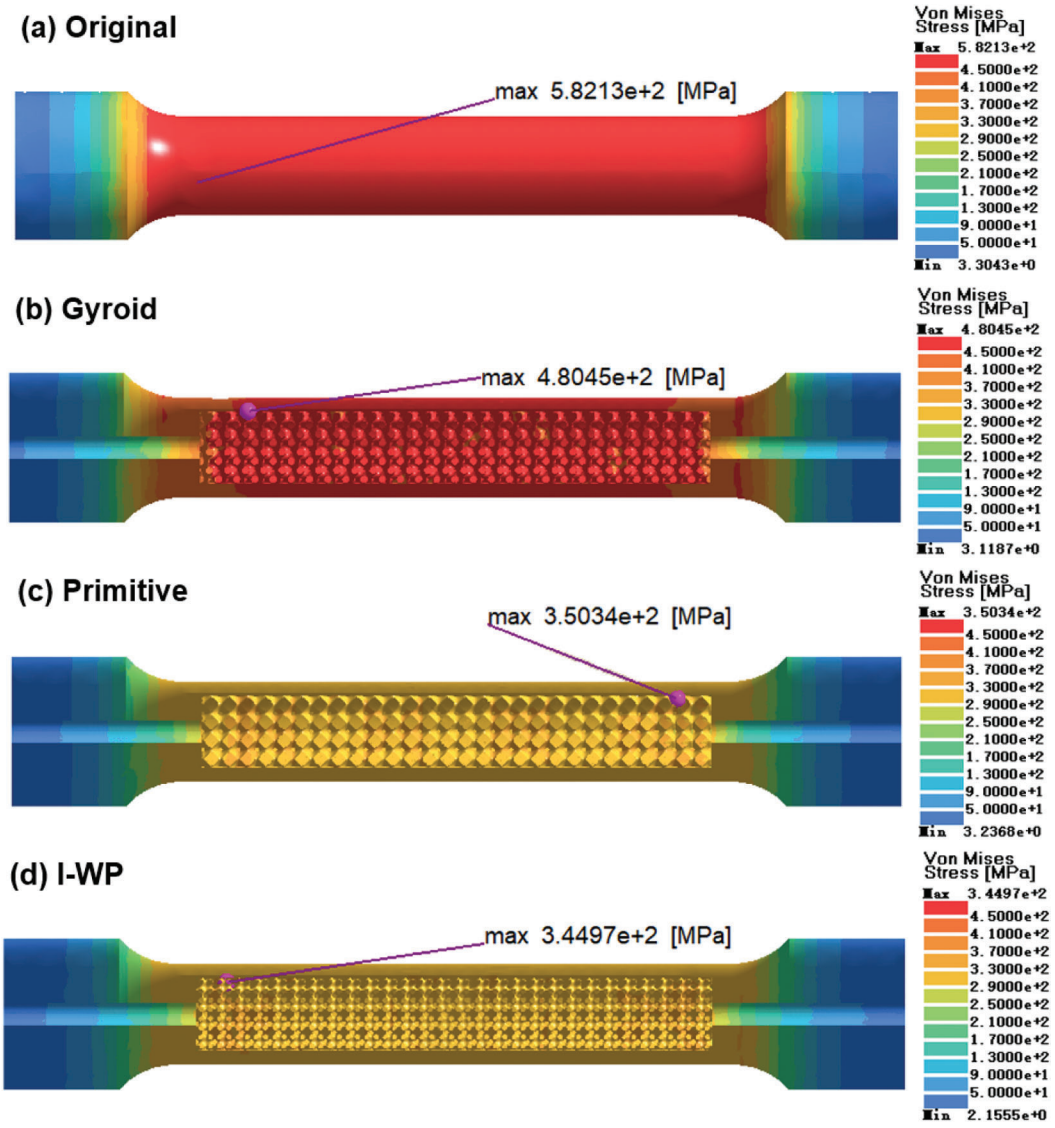

Figure 4: Von Mises stress distribution in finite element tensile simulations of the solid, Gyroid, Primitive, and I-WP test pieces

effective total strain of the TPMS porous test piece, which does not include the strain that occurs in the transition section, clamping section, and test fixture under a tensile load. It should not be confused with the local strain of the TPMS unit cell. Similarly, the ordinate axis 'stress' is the effective stress of the entire structure, which is obtained by applying the load divided by the original cross-sectional area (78.5 mm^2) of the test piece and is not related to the local stress in the TPMS unit cell. Since the research of Gibson, Ashby et al. [24], this method has been used to analyse porous structures as it can directly identify the key features of structural deformation.

It is clear from the stress-strain curve in Fig. 6a that the solid test piece first passed through the stage of elastic deformation and subsequently entered the stage of deformation strengthening. After reaching the tensile strength limit, necking appeared, the curve showed a downward trend and subsequently fracture occurred, and the yield platform effect was not obvious. The stress-strain curves of TPMS porous test pieces did not exhibit an obvious plastic deformation strengthening zone, and they broke immediately

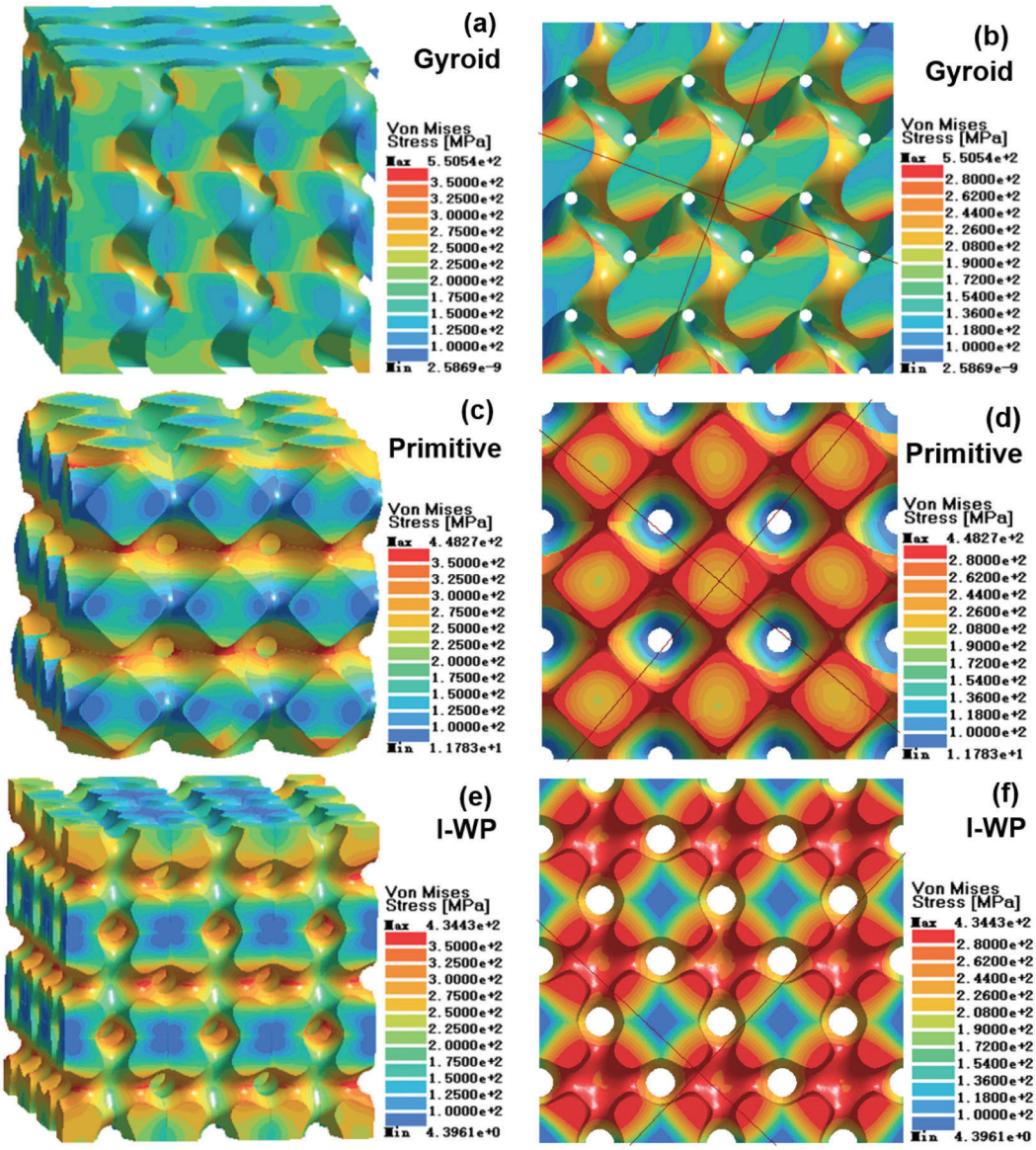

Figure 5: Overall and section von Mises stress distributions in finite element tensile simulations of the Gyroid, Primitive, and I-WP unit cell array of 3 × 3 × 3 lattice

after reaching the tensile strength limit. Fig. 6b shows the fracture position of each TPMS porous test piece after the tensile test. As shown, the fracture positions of the three types of porous test pieces appear near the clamping end (the end of the powder hole), which is consistent with the prediction results of finite element simulations. Combined with the simulation results, it is clear that a stress concentration is likely to occur at the junction of the porous structure and the shell of the test piece, and the stress distribution in the transition from the porous structure to the solid clamping part is uneven, which results in the consistent fracture position of the porous test piece. Hence, the type of porous unit cell is not a contributing factor.

By measuring the elongation and section diameter after fracture, the percentage elongation and the percentage of reduced area of the solid and TPMS porous test pieces can be calculated. Tab. 3 shows the yield strength and tensile strength of each test piece.

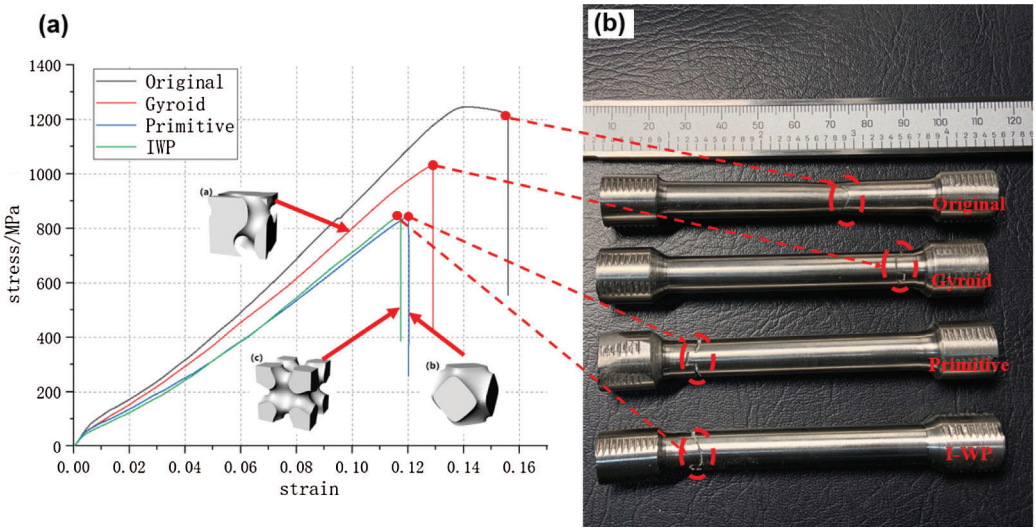

Figure 6: 6a shows the stress-strain curve of the solid and TPMS porous test pieces. Among them, the black, red, blue, and green curves represent the stress-strain curves of the Original, Gyroid, Primitive, and I-WP test pieces, respectively, and the corresponding geometric model of the unit cell is provided. The location of the test piece fracture is shown in Fig. 6b

Table 3: Summary of characteristic parameters of the solid, Gyroid, Primitive, and I-WP porous tensile test pieces

Specimen name	Yield strength σ_s/MPa	Tensile strength σ_b/MPa	Percentage elongation	Percentage reduced area
Original	1148.2 ± 38.1	1235.3 ± 16.8	11.81% ± 1.37%	20.96% ± 3.68%
Gyroid	979.7 ± 19.8	1017.1 ± 17.1	3.78% ± 0.56%	2.13% ± 0.30%
Primitive	830.9 ± 15.5	858.7 ± 14.9	3.76% ± 0.35%	1.59% ± 0.21%
I-WP	803.8 ± 25.6	824.1 ± 27.4	4.09% ± 0.88%	2.46% ± 0.41%

As shown from the table above, compared with the solid test pieces, the average tensile strengths of the Gyroid, Primitive, and I-WP porous test pieces decreased by 17.7%, 30.5%, and 33.3%, respectively, and the average yield strength decreased by 14.7%, 27.6%, and 30.0%, respectively. Among them, the tensile strength of the solid test pieces manufactured by SLM reached 1235 MPa, which was a significant improvement over the tensile strength of test pieces manufactured by traditional casting and forging processes. This is because the cooling rate during SLM manufacturing is extremely high, and the grains formed after the powder solidifies are fine, thereby affording test pieces of higher tensile strength.

Among the three TPMS porous test pieces, the tensile strength of the Gyroid test piece was the highest, which is consistent with the finite element simulation results. This shows that the Simsolid simulation experiment has a certain reference value. The linear elastic finite element analysis performed in this study can only qualitatively provide the performance differences of porous test pieces and cannot provide more accurate values such as the yield strength and tensile strength to compare with the experimental results. If more accurate quantitative simulation results are desired, then nonlinear finite element analysis should be performed by importing the standard tensile experimental data of the Ti6Al4V solid test piece manufactured by SLM. Additionally, from the tensile test results, no necking occurred in the porous test

pieces, and the yield and tensile strengths were basically the same, as reflected in the stress-strain curve in Fig. 6a and the fracture test piece in Fig. 6b and Tab. 3.

4.3 Fracture Analysis

The macroscopic shape of the fracture surface of the solid test piece is 'cupped cone', and the shear lip forms an included angle of 45° with the applied tensile stress. From the microscopic appearance, the fracture surface is divided into two regions, including a ductile fracture region with a rectangular middle and a cleavage region at the edge, as shown in Fig. 7b. Clear cleavage steps and tearing edges can be observed in the cleavage area, and river-like patterns with fewer tributaries appeared, as shown in Fig. 7a. Furthermore, observing the micromorphology of the ductile fracture area, it is clear that a large number of equiaxed dimples appeared in Fig. 7c, and that large dimples nested with small dimples. The size of the dimples varied from several to several tens of microns, indicating that the solid test piece exhibited a certain degree of plasticity although the toughness distribution was uneven.

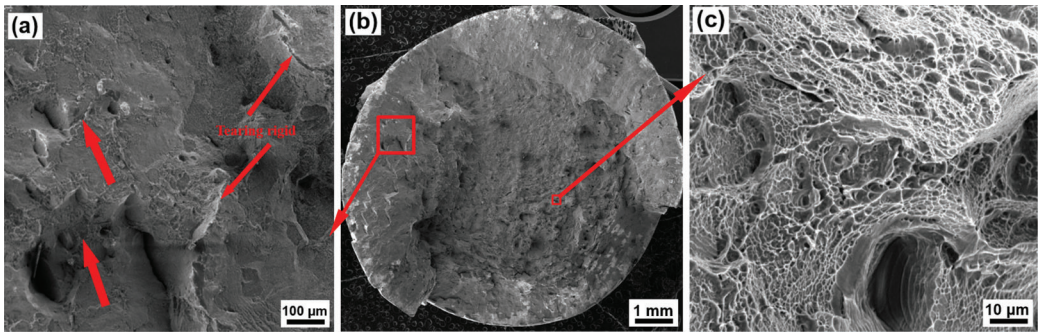

Figure 7: 7b shows the complete fracture morphology of solid tensile test pieces; 7a and 7c show cleavage and ductile fracture characteristics of solid tensile test pieces, respectively

In Fig. 8a, the fracture surface of the Gyroid porous test piece is divided into three regions, including dark grey 'corrugated' pore regions formed by porous unit cell arrays in the central region, unit cell fracture surfaces, and shear lips at the edges. The fracture morphology of the Primitive and I-WP test pieces has a similar regional distribution to Gyroid, in which the Primitive pore region is 'spherical', while the I-WP pore region is 'cross', as shown in Figs. 8c and 8e, respectively. A large amount of unmelted or semi-melted powder appeared in the pore region, which was caused by the low moving speed of laser scanning of the porous structure edges and the long existence time of the molten pool, such that the liquid molten pool 'devours' the surrounding powder bed to form the edge powder adhering effect. This phenomenon affects the forming precision and mechanical properties of the porous structure. The edge shear lips of the three types of porous test pieces show similar cleavage fracture microscopic characteristics as those of the solid test pieces, which will not be repeated herein.

As shown in Fig. 8b, the fracture surface of the Gyroid unit cell is in the shape of an inward depression, which indicates that the unit cell has undergone torsional deformation. The fracture surface is at an angle of approximately 45° with the tensile direction, thereby indicating that shear force is applied. Based on the 'spiral' geometric characteristics of the Gyroid unit cell, it is clear that the axial tensile force, owing to the excellent geometric characteristics of the Gyroid unit cell, is decomposed and generates shear forces and torques during the tensile test, which render the unit cell more uniform in force. Hence, the tensile strength of the Gyroid porous test piece is higher than those of the other two structures. As shown in Fig. 8d, the fracture surface of the Primitive unit cell is at a 90° angle with the tensile load direction, indicating that the unit cell is only subjected to an axial tensile force. The periphery of the fracture

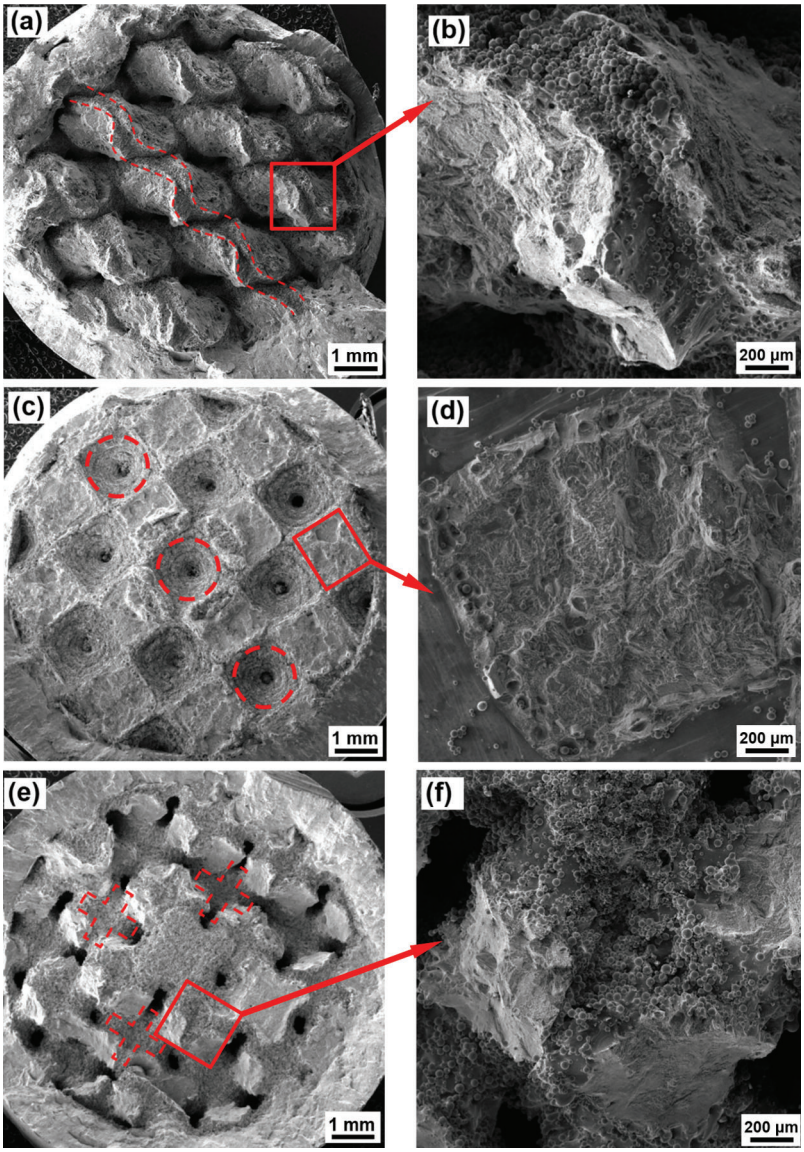

Figure 8: 8a, 8c, and 8e show the complete fracture morphology of Gyroid, Primitive, and I-WP porous test pieces. The fracture morphologies of the filled cell in the porous test piece are shown in Figs. 8b, 8d, and 8f. In particular, 8d shows the micromorphology of the unit cell in the corresponding area of the other half of the marked area

surface is smooth and flat, which is the solid surface at the end of the gauge segment of the test piece. This indicates that the fracture of the Primitive test piece occurred in the narrow neck area of the unit cell at the end of the gauge section. Furthermore, the finite element simulation experiment verified that the area is prone to stress concentration. The experimental and simulation results are consistent. As shown in Fig. 8f, the fracture surface of the I-WP unit cell is at an angle of approximately 45° with the tensile direction, indicating that the tensile load is partially decomposed into shear forces, and the fracture position is consistent with the stress concentration position in the finite element simulation experiment, i.e., it occurs in the thin column area of its own structure.

The results of this study avoid the need for a large number of finite element simulations and mechanical performance tests of TPMS porous structures and can be used as a good reference for the internal structure selection of regenerative cooling structures. Although this study provided invaluable results, many deficiencies still exist. For example, the finite element simulation was limited to qualitative analysis and could not be further compared with the results of tensile experiments. The experimental variables were relatively single, and only the mechanical properties of different structures with a single porosity were studied. Furthermore, bionic structure design is not closely related to the specific load-carrying structure of the aircraft. The following can be performed as future work: first, a non-linear static finite element simulation analysis can be performed. Subsequently, a series of studies regarding the properties of TPMS porous structures with different porosities can be performed along with heat treatment [25] to form a comprehensive selection library of porous unit cells. Furthermore, research on the heat transfer performance of porous unit cells can be conducted to ensure the maximum function of the regenerative cooling structure [26]. These studies will benefit aerospace and other fields such as biomedicine.

5 Conclusion

In this paper, the selection of porous unit cells in a regenerative cooling structure was studied. With Ti6Al4V as the material, porous test pieces filled with Gyroid, Primitive, and I-WP unit cells with 30% porosity and solid test pieces were designed and manufactured. The mechanical response of these structures under a tensile load was studied through finite element simulation and experiment. Furthermore, a SEM micrograph analysis of the fracture surface of the test piece was performed. The conclusions of this study are as follows:

1. The quality of the Gyroid, Primitive and I-WP porous test pieces decreased by 8.21%, 5.66%, and 8.45%, respectively, compared with that of the solid test pieces. Owing to the micro-scale pores appearing in the array of the Primitive sample, some of the powder could not be removed, and the mass was greater than those of the other two structures.
2. In the tensile test, the average tensile strength of the Gyroid, Primitive, and I-WP porous specimens decreased by 17.7%, 30.5%, and 33.3%, respectively, compared with that of the solid test pieces. Necking was not observed. The results of finite element simulation and tensile test demonstrated that among the three TPMS porous unit cells, Gyroid exhibited better mechanical properties and was more suitable for the internal porous structure design of the regenerative cooling structure.
3. The results of finite element simulation demonstrated that the stress distribution of the Gyroid unit cell was more uniform, and that stress concentration could occur easily in the Primitive unit cell at the thin neck area where the element was connected, while the stress of the I-WP unit cell was primarily concentrated at the thin column of the element. According to the fracture morphology of the porous test piece, the Gyroid unit cell was subjected to the joint action of axial tension, shear force, and torque in the tensile test, the Primitive unit cell was only subjected to axial load, while the I-WP unit cell was subjected to axial tension and shear force. The Gyroid unit cell exhibited the better mechanical conductivity.

Acknowledgement: The authors are thankful for the support from the National Natural Science Foundation of China (NSFC, Project Nos. 91860136 and 51801231), the Key R&D Plan of Guangdong Province (Grant No. 2018B090905001) and the Key Science and Technology project of Shaanxi Province (Grant No. 2018zdzx01-04-01).

Conflicts of Interest: The authors declare that they have no conflicts of interest to report regarding the present study.

Funding Statement: This research was funded by the National Natural Science Foundation of China (Nos. 91860136 and 51801231), the Key R&D Plan of Guangdong Province (Grant No. 2018B090905001) and the Key Science and Technology project of Shaanxi Province (Grant No. 2018zdzx01-04-01). The authors would like to thank for these financial supports.

References

1. Zhang, S. L., Qin, J., Zhou, W. X., Bao, W. (2018). Review of research on regenerative cooling in hypersonic propulsion. *Journal of Propulsion Technology, 39(10),* 23–36.
2. Ma, L., Yang, J. J., Zhang, W. G. (2012). Overview of the development of hypersonic vehicles. *Aircraft Missiles, 6,* 26–31.
3. Brockmeyer, J., Fortini, A., Williams, B., Tuffias, R. (2013). High-efficiency open-cell foam heat exchangers for actively cooled propulsion components. *AIAA/ASME/SAE/ASEE Joint Propulsion Conference & Exhibit, Cleveland, OH, USA*. DOI 10.2514/6.1998-3441.
4. Chung, J., Tully, L., Kim, J. H., Jones, G., Watkins, W. (2013). Evaluation of open cell foam heat transfer enhancement for liquid rocket engine. *AIAA/ASME/SAE/ASEE Joint Propulsion Conference & Exhibit, Sacramento, California, USA*. DOI 10.2514/6.2006-5050
5. Ma, S., Tang, Q., Feng, Q. X., Song, J., Han, X. X. et al. (2019). Mechanical behaviours and mass transport properties of bone-mimicking scaffolds consisted of gyroid structures manufactured using selective laser melting. *Journal of the Mechanical Behavior of Biomedical Materials, 93,* 158–169. DOI 10.1016/j.jmbbm.2019.01.023.
6. Gorny, B., Niendorf, T., Lackmann, J., Thoene, M., Troester, T. et al. (2011). In situ characterization of the deformation and failure behavior of non-stochastic porous structures processed by selective laser melting. *Material Science and Engineering: A, 528(27),* 7962–7967. DOI 10.1016/j.msea.2011.07.026.
7. Rakow, J. F., Waas, A. M. (2005). Thermal buckling of metal foam sandwich panels for convective thermal protection systems. *Journal of Spacecraft and Rockets, 42(5),* 832–844. DOI 10.2514/1.9741.
8. Wang, D., Wang, Y. M., Yang, Y. Q., Lu, J. B., Xu, Z. L. et al. (2019). Research on design optimization and manufacturing of coating pipes for automobile seal based on selective laser melting. *Journal of Materials Processing Tech, 273,* 116–227.
9. Mohammad, K., Henning, R. (2017). Modeling of processing-induced pore morphology in an additively-manufactured Ti-6Al-4V alloy. *Materials, 10(2),* 145–159. DOI 10.3390/ma10020211.
10. Peng, W. M., Liu, Y. F., Jiang, X. F., Dong, X. T., Jun, J. et al. (2019). Bionic mechanical design and 3D printing of novel porous Ti6Al4V implants for biomedical applications. *Journal of Zhejiang University-SCIENCE B, 20(8),* 647–659. DOI 10.1631/jzus.B1800622.
11. Arabnejad, S., Johnston, R. B., Pura, J. A., Singh, B., Tanzer, M. et al. (2016). High-strength porous biomaterials for bone replacement: a strategy to assess the interplay between cell morphology, mechanical properties, bone ingrowth and manufacturing constraints. *Acta Biomaterialia, 30,* 345–356. DOI 10.1016/j.actbio.2015.10.048.
12. Zhang, P. Y., Zhou, X., Cheng, X., Sun, H. M., Ma, H. Q. et al. (2020). Elucidation of bubble evolution and defect formation in directed energy deposition based on direct observation. *Additive Manufacturing, 32,* 101026. DOI 10.1016/j.addma.2019.101026.
13. Huang, W. D. (2007). *Laser stereforming*. Xi'an, Shaanxi: Northwestern Polytechnical University Press.
14. Beharic, A., Egui, R. R., Yang, L. (2018). Drop-weight impact characteristics of additively manufactured sandwich structures with different cellular designs. *Materials & Design, 145,* 122–134. DOI 10.1016/j.matdes.2018.02.066.
15. Tian, J., Lu, T. J., Hodson, H. P., Queheillalt, D. T., Wadley, H. N. G. (2007). Cross flow heat exchange of textile cellular metal core sandwich panels. *International Journal of Heat and Mass Transfer, 50(13-14),* 2521–2536. DOI 10.1016/j.ijheatmasstransfer.2006.11.042.
16. Yan, C. Z., Hao, L., Hussein, A., Young, P., Raymont, D. (2014). Advanced lightweight 316L stainless steel cellular lattice structures fabricated via selective laser melting. *Materials & Design, 55,* 533–541. DOI 10.1016/j.matdes.2013.10.027.

17. Rossman, W. (2005). Infinite periodic discrete minimal surfaces without self-intersections. *Balkan Journal of Geometry & Its Applications, 10(2),* 106–128.
18. Bidan, C. M., Wang, F. M., Dunlop, J. W. C. (2013). A three-dimensional model for tissue deposition on complex surfaces. *Computer Methods in Biomechanics and Biomedical Engineering, 16(10),* 1056–1070. DOI 10.1080/10255842.2013.774384.
19. Yoo, D. J. (2014). Advanced porous scaffold design using multi-void triply periodic minimal surface models with high surface area to volume ratios. *International Journal of Precision Engineering and Manufacturing, 15(8),* 1657–1666. DOI 10.1007/s12541-014-0516-5.
20. Maskery, I., Sturm, L., Aremu, A. O., Panesar, A., Williams, C. B. et al. (2018). Insights into the mechanical properties of several triply periodic minimal surface lattice structures made by polymer additive manufacturing. *Polymer, 152,* 62–71. DOI 10.1016/j.polymer.2017.11.049.
21. Wang, D., Wu, S. B., Bai, Y. C., Lin, H., Yang, Y. Q. et al. (2017). Characteristics of typical geometrical features shaped by selective laser melting. *Journal of Laser Applications, 29(2),* 022007. DOI 10.2351/1.4980164.
22. ISO6892-1. (2009). Metallic material-Tensile testing-Part1: method of test at room temperature. 2009 MOD.
23. Gümrük, R., Mines, R. A. W., Karadeniz, S. (2013). Static mechanical behaviours of stainless steel micro-lattice structures under different loading conditions. *Materials Science & Engineering A, 586,* 392–406. DOI 10.1016/j.msea.2013.07.070.
24. Gibson, L., Ashby, M. (1997). *Cellular solids: structure and properties*. UK: Cambridge University Press.
25. Zhang, M. K., Yang, Y. Q., Wang, D., Xiao, Z. F., Song, C. H. et al. (2018). Effect of heat treatment on the microstructure and mechanical properties of Ti6Al4V gradient structures manufactured by selective laser melting. *Materials Science and Engineering A, 736,* 288–297. DOI 10.1016/j.msea.2018.08.084.
26. Huang, R. X., Tan, Y. H., Liu, J. Y., Yang, B. E. (2019). Thermal analysis method on complex regenerative cooling structure in supersonic flows. *Journal of Propulsion Technology, 40(2),* 376–381.